Electronic Supplementary Material (ESI) for Journal of Materials Chemistry A.

Supporting Information

General and Precise Carbon Confinement of Functional Nanostructures Derived from Assembled Metal-Phenolic Network for Enhanced Lithium Storage

Zhitong Xiao, Jiashen Meng, Qi Li* Xiao Zhang, Ziang Liu, Bo Wen, Chunhua Han and Liqiang Mai*

State Key Laboratory of Advanced Technology for Materials Synthesis and Processing, International School of Materials Science and Engineering, Wuhan University of Technology, Luoshi Road 122, Wuhan, 430070, Hubei, China.

*E-mail: qi.li@whut.edu.cn; mlq518@whut.edu.cn

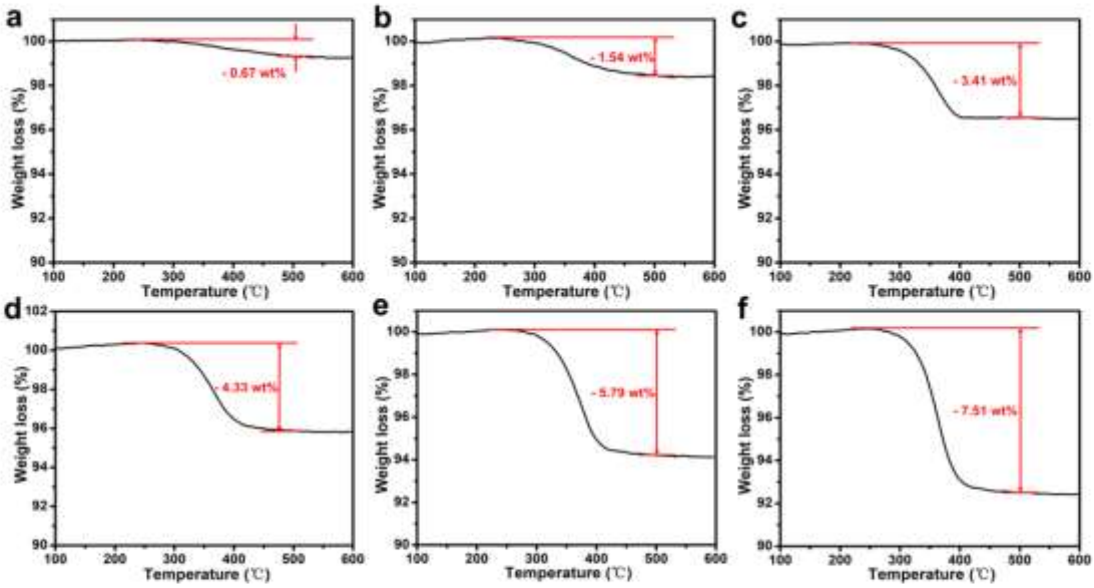

Fig. S1 (a-f) TG curves of SnO_2@C-Fe_2O_3-1, SnO_2@C-Fe_2O_3-3, SnO_2@C-Fe_2O_3-7, SnO_2@C-Fe_2O_3-10, SnO_2@C-Fe_2O_3-15 and SnO_2@C-Fe_2O_3-20, respectively, in air at 10 °C min^{-1}.

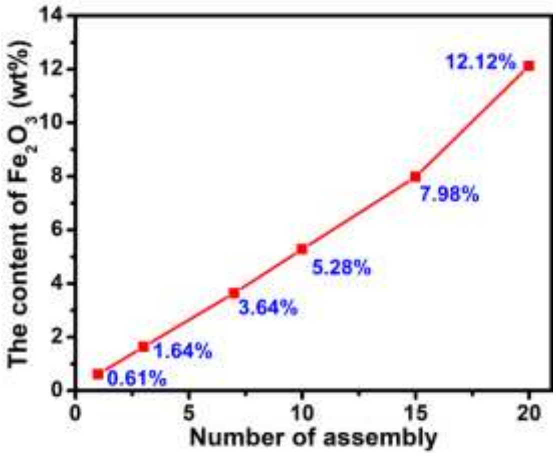

Fig. S2 The relationship between the content of Fe_2O_3 and the number of assembly layer according to the ICP results.

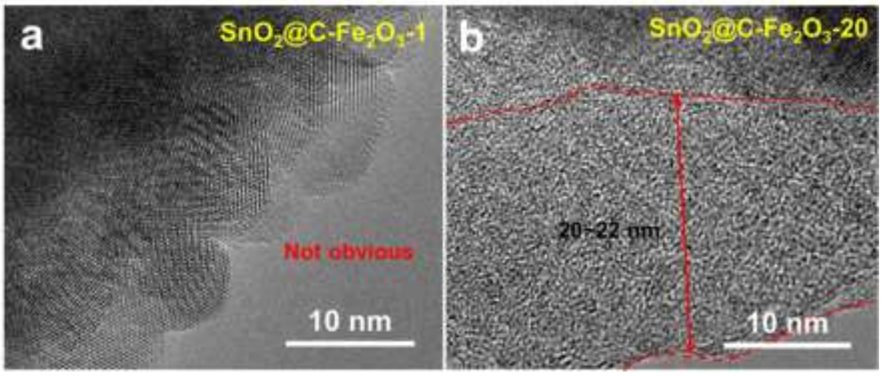

Fig. S3 (a, b) HRTEM images of SnO_2@C-Fe_2O_3-1 and SnO_2@C-Fe_2O_3-20, respectively.

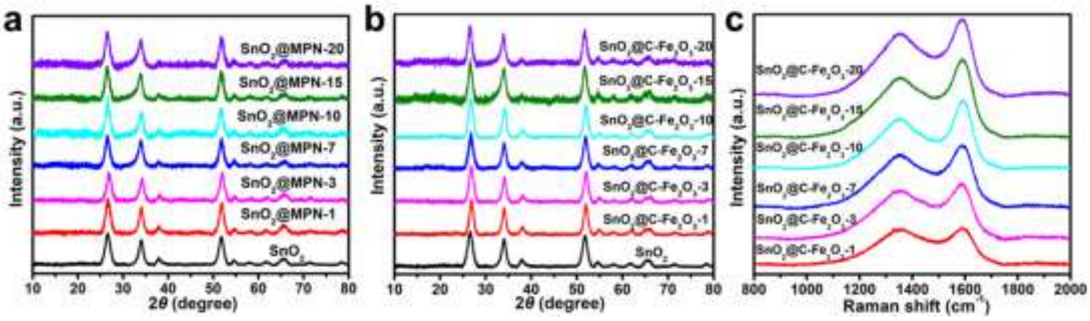

Fig. S4 (a) XRD patterns of SnO_2, SnO_2@MPN-1, SnO_2@MPN-3, SnO_2@MPN-7, SnO_2@MPN-10, SnO_2@MPN-15 and SnO_2@MPN-20. (b) XRD patterns of SnO_2, SnO_2@C-Fe_2O_3-1, SnO_2@C-Fe_2O_3-3, SnO_2@C-Fe_2O_3-7, SnO_2@C-Fe_2O_3-10, SnO_2@C-Fe_2O_3-15 and SnO_2@C-Fe_2O_3-20. (c) Raman spectra of SnO_2@C-Fe_2O_3-1, SnO_2@C-Fe_2O_3-3, SnO_2@C-Fe_2O_3-7, SnO_2@C-Fe_2O_3-10, SnO_2@C-Fe_2O_3-15 and SnO_2@C-Fe_2O_3-20.

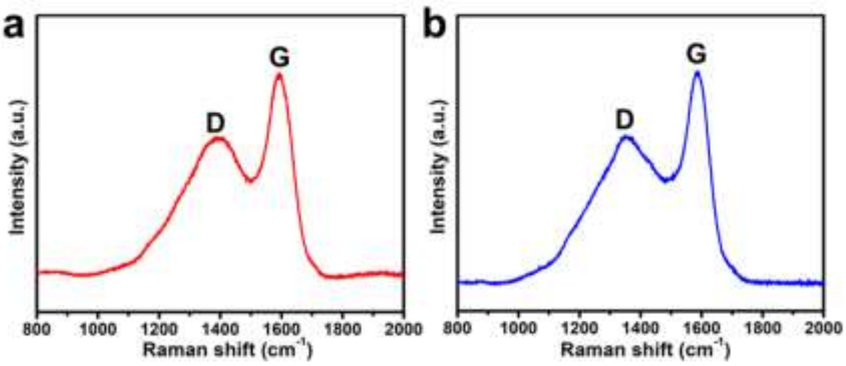

Fig. S5 (a, b) Raman spectra of the pure carbon derived from gallic acid and pyrogallic acid, respectively.

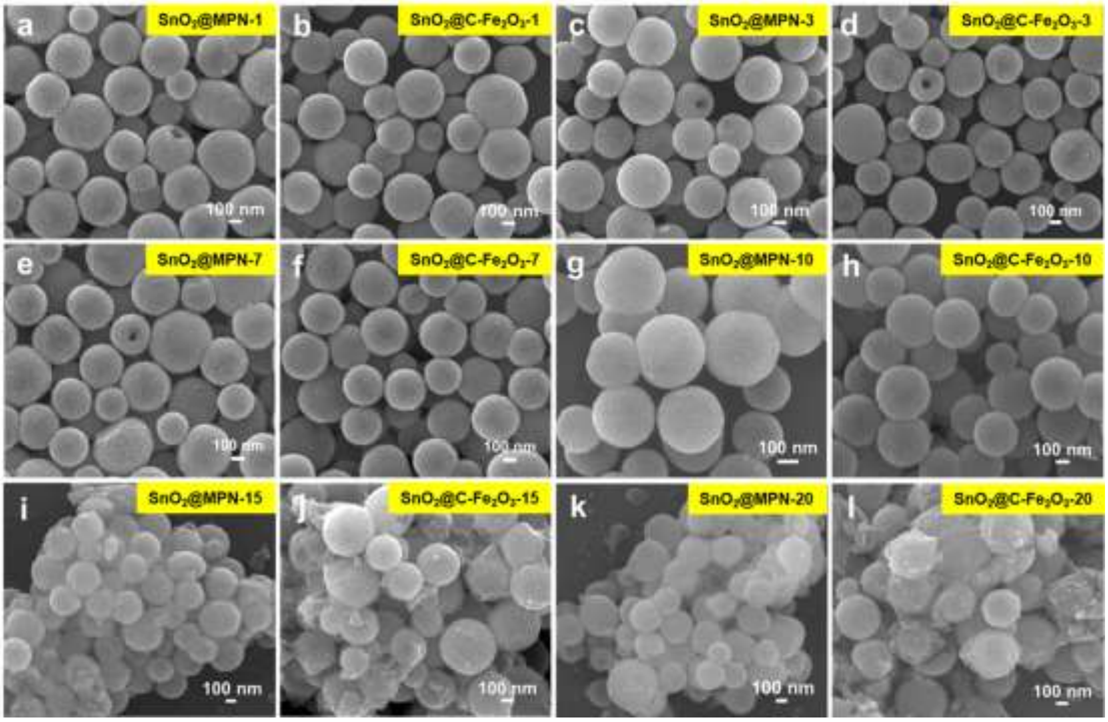

Fig. S6 (a, c, e, g, i and k) SEM images of SnO_2@MPN-1, SnO_2@MPN-3, SnO_2@MPN-7, SnO_2@MPN-10, SnO_2@MPN-15 and SnO_2@MPN-20, respectively. (b, d, f, h, j and l) SEM images of SnO_2@C-Fe_2O_3-1, SnO_2@C-Fe_2O_3-3, SnO_2@C-Fe_2O_3-7, SnO_2@C-Fe_2O_3-10, SnO_2@C-Fe_2O_3-15 and SnO_2@C-Fe_2O_3-20, respectively.

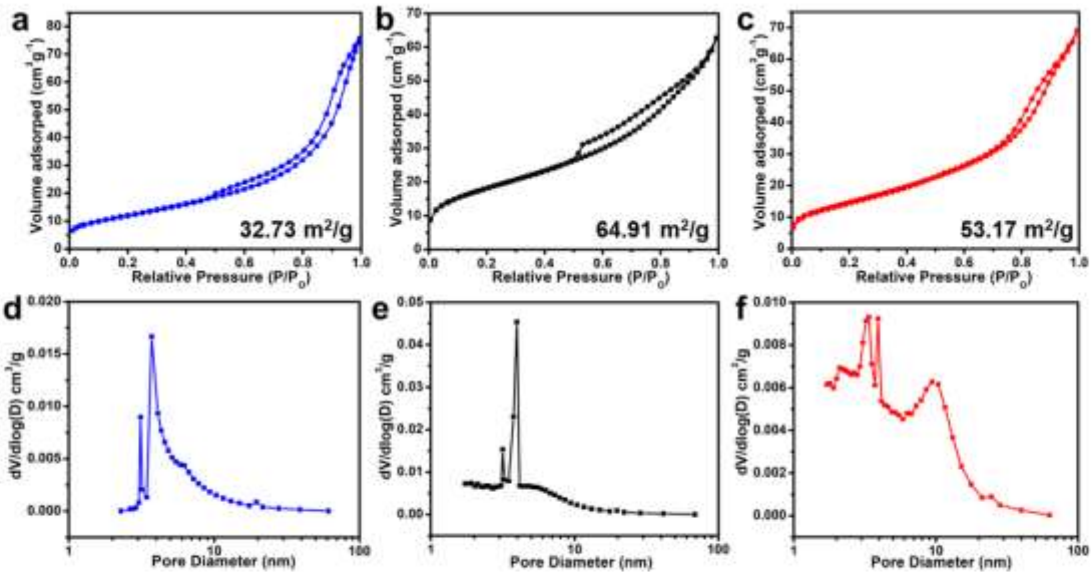

Fig. S7 (a, d) N_2 adsorption/desorption isotherm and the corresponding pore size distribution of SnO_2, respectively. (b, e) N_2 adsorption/desorption isotherm and the corresponding pore size distribution of SnO_2@MPN-10, respectively. (c, f) N_2

adsorption/desorption isotherm and the corresponding pore size distribution of SnO_2@C-Fe_2O_3-10, respectively.

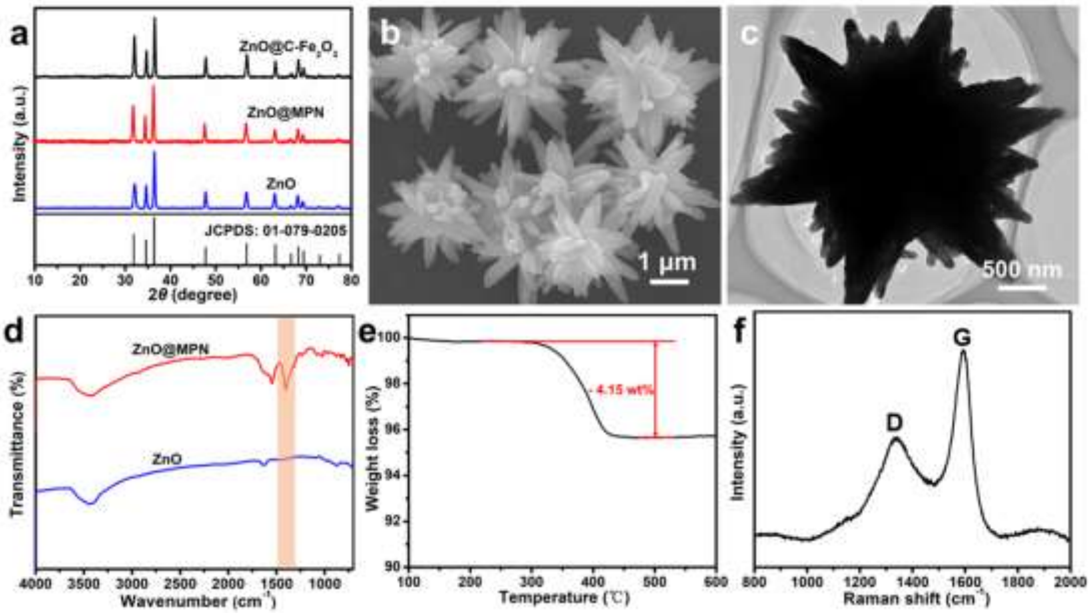

Fig. S8 (a) XRD patterns of ZnO, ZnO@MPN and ZnO@C-Fe_2O_3 microflowers. (b, c) SEM and TEM images of ZnO microflowers, respectively. (d) FT-IR spectra of ZnO and ZnO@MPN. (e, f) TG curve and Raman spectrum of ZnO@C-Fe_2O_3, respectively.

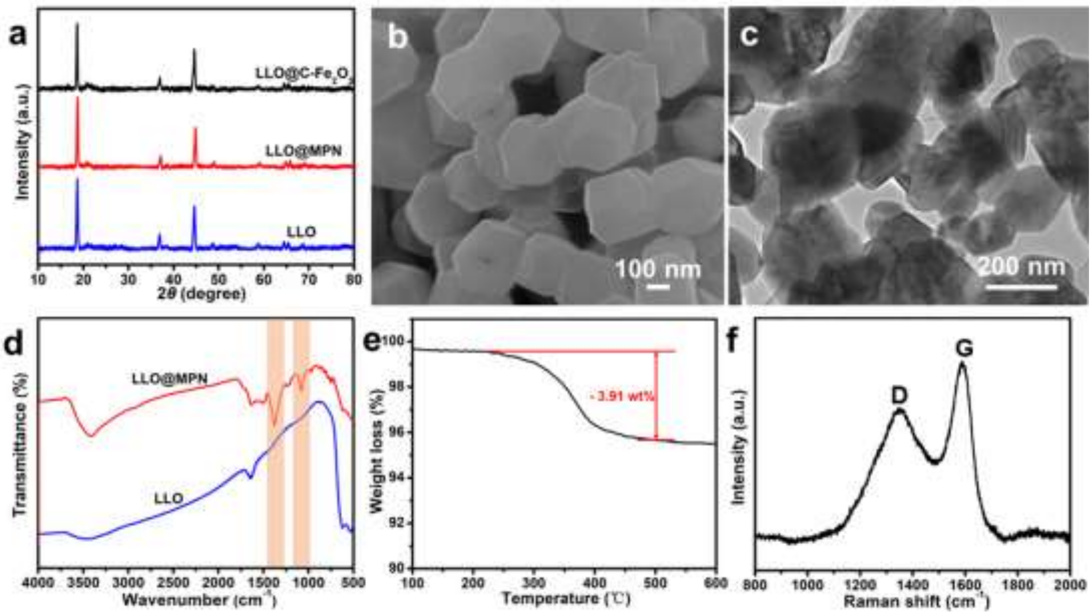

Fig. S9 (a) XRD patterns of LLO, LLO@MPN and LLO@C-Fe_2O_3 nanoparticles. (b, c) SEM and TEM images of LLO nanoparticles, respectively. (d) FT-IR spectra of LLO and LLO@MPN. (e, f) TG curve and Raman spectrum of LLO@C-Fe_2O_3, respectively.

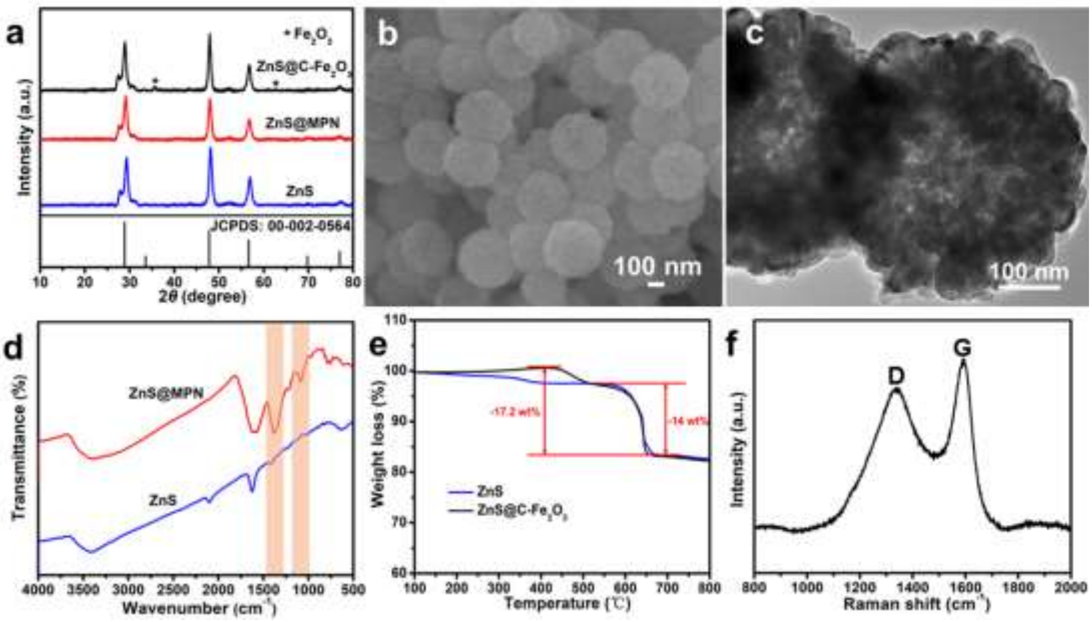

Fig. S10 (a) XRD patterns of ZnS, ZnS@MPN and ZnS@C-Fe_2O_3 hollow spheres. (b, c) SEM and TEM images of ZnS hollow spheres, respectively. (d) FT-IR spectra of ZnS and ZnS@MPN. (e, f) TG curve and Raman spectrum of ZnS@C-Fe_2O_3, respectively.

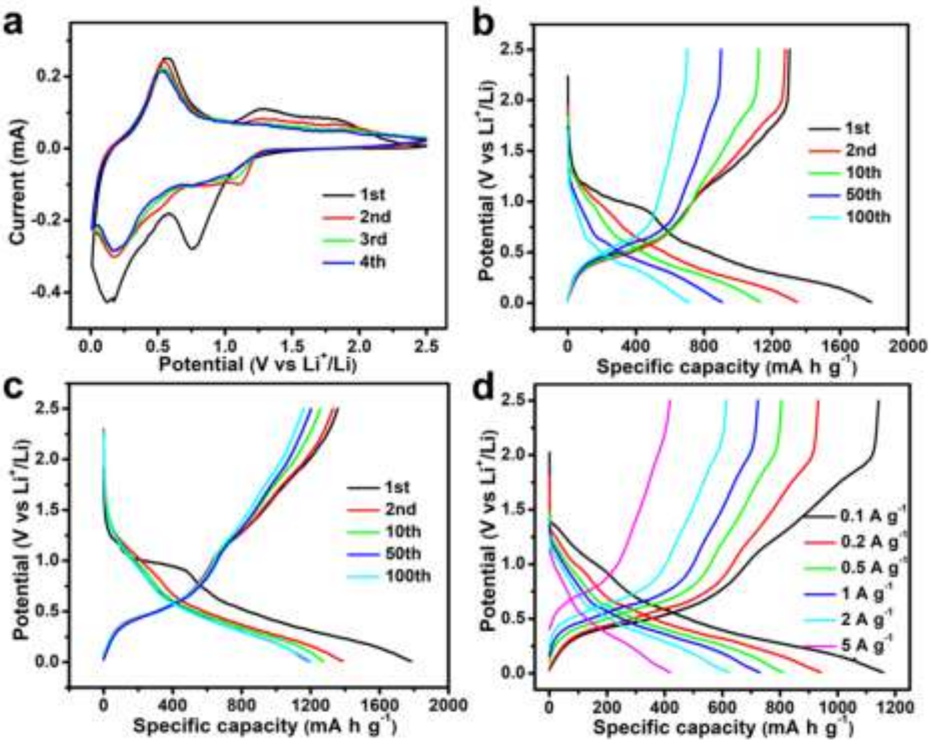

Fig. S11 (a) CV curves of the first four cycles at the scan rate of 0.2 mV s^{-1} of SnO_2 in the 0.01-2.5 V range. (b, c) Charge-discharge curves (for the 1st, 2nd, 10th, 50th and

100th cycle at the rate of 0.2 A g^{-1}) of SnO_2 and SnO_2@C-Fe_2O_3-10, respectively. (d) The charge-discharge voltage profiles of the SnO_2 at different current densities.

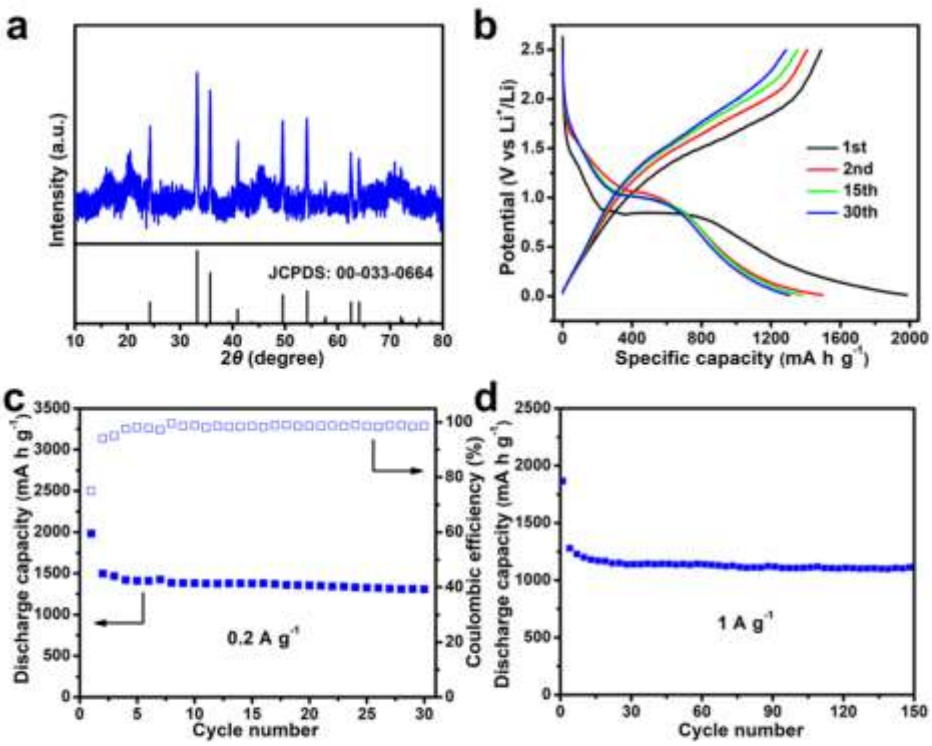

Fig. S12 (a) XRD patterns of the C-Fe_2O_3 derived from pure MPN. (b) Charge-discharge curves (for the 1st, 2nd, 15th and 30th cycle at 0.2 A g^{-1}) of C-Fe_2O_3. (c) Cycling performance and the corresponding Coulombic efficiencies of C-Fe_2O_3 at 0.2 A g^{-1}. (d) Long-term cycling performance of C-Fe_2O_3 at 1 A g^{-1}.

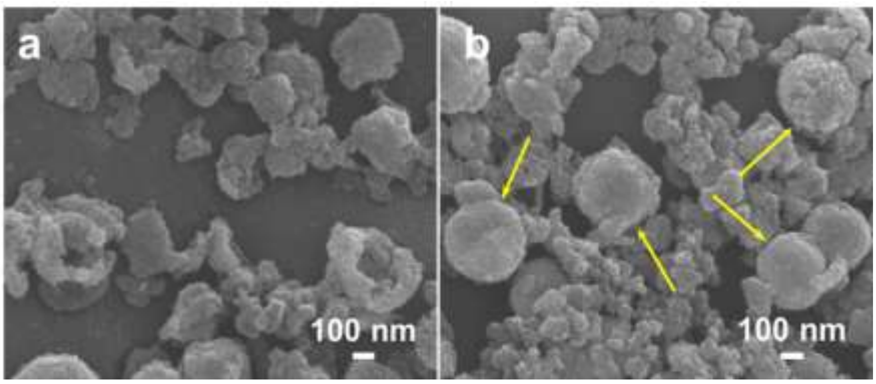

Fig. S13 (a, b) SEM images after 100 cycles at 0.2 A g^{-1} for SnO_2 and SnO_2@C-Fe_2O_3-10, respectively.

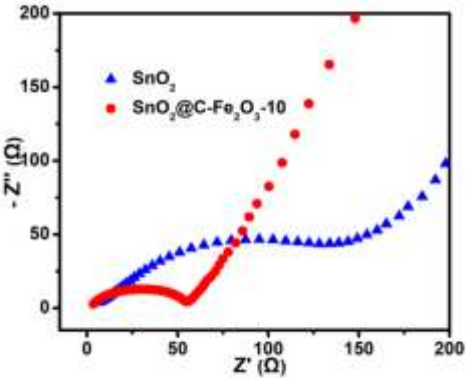

Fig. S14 Nyquist plots measured at 2.5 V in the frequency range of 100 kHz-0.01 Hz.

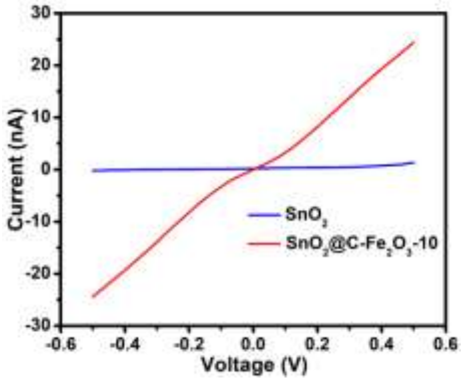

Fig. S15 I-V curves of SnO_2 and SnO_2@C-Fe_2O_3-10.

Table S1. The ICP test results of the SnO_2@C-Fe_2O_3-1, SnO_2@C-Fe_2O_3-3, SnO_2@C-Fe_2O_3-7, SnO_2@C-Fe_2O_3-10, SnO_2@C-Fe_2O_3-15 and SnO_2@C-Fe_2O_3-20.

Material	**Sn : Fe**	**The content of Fe_2O_3 (wt%)**
SnO_2@C-Fe_2O_3-1	0.9942 : 0.0058	0.61
SnO_2@C-Fe_2O_3-3	0.9843 : 0.0157	1.64
SnO_2@C-Fe_2O_3-7	0.9644 : 0.0356	3.64
SnO_2@C-Fe_2O_3-10	0.9477 : 0.0523	5.28
SnO_2@C-Fe_2O_3-15	0.9496 : 0.0804	7.98
SnO_2@C-Fe_2O_3-20	0.8754 : 0.1246	12.12

Table S2. A comparison of our work and conventional carbon coating methods.

Coating methods	**Coating sources**	**Advantages**	**Disadvantages**	**References**
Metal-phenolic network modification	**MPN**	**● Precise control** **● Simple and fast manipulation** **● Programmable process** **● No substrate selectivity** **● Low cost**	**● Solvent consuming**	**Our work**
Solution-based polymerization	Dopamine	● Simple manipulation ● Low cost ● No substrate selectivity	● Solvent consuming ● Tedious synthesis process ● Hard control on uniform coatings	*Adv. Mater.* 2017, **29**, 1700989.
Low-pressure vapor superassembly	MOFs	● No solvent consuming ● Low cost ● Simple manipulation	● Substrate material selectivity ● Hard control on precise coatings	*Nano Lett.* 2017, **17**, 7773-7781.

			● Some requirements of operation condition	
Sol-gel method	Citric acid	● Simple manipulation ● Low cost ● No substrate selectivity	● Hard control on uniform coatings ● Solvent consuming ● Tedious synthesis process	*J. Alloys Compd.*2011, **509**, 712-718.
Chemical vapor deposition	Carbon	● Precise control ● Uniform deposition ● High quality coatings	● Complex manipulation ● High cost ● High requirements of operation condition	*J. Mater. Chem.* 2010, **20**, 595-602.
Atomic layer deposition	Metal organic compounds	● Uniform and conformal deposition ● High quality coatings ● Precise control	● High cost ● Complex manipulation ● High requirements of operation condition	*Energy Environ. Sci.*, 2012, **5**, 6872-6879.

Table S3. Electrochemical performance comparison of various modified SnO_2 anode.

SnO_2 anode	**Voltage range (V)**	**Current density (mA g^{-1})**	**Cycle number**	**Residual capacity (mA h g^{-1})**	**Capacity retention**	**Reference**
SnO_2@C-Fe_2O_3-10	**0.01-2.5**	**200 1000**	**100 1000**	**1203 1003**	**91 % 86 %**	**Our work**
Hollow structured SnO_2@Si nanospheres	0.01-1	300	500	778	86 %	S1
RGO/SnO_2 composites	0.01-2	100	200	718	79 %	S2
Silver nanoparticle-decorated SnO_2/NiO nanotubes	0.01-3	1000	500	826	81 %	S3
rGO enwrapping hollow SnO_2 nanospheres	0.01-3	100	100	1107	82 %	S4
Sandwiched C@SnO_2@C hollow structures	0.005-3	100	50	933	93 %	S5
Ultrafine SnO_2/graphene nanocomposite	0.01-3	1000	230	970	97 %	S6
SnO_2@Fe_2O_3 sandwich cubes	0.01-3	100	200	750.8	83 %	S7

Carbon coated SnO_2 nanoparticles anchored on CNT	0.01-2.5	1000	150	930	81 %	S8
Okra-like SnO_2 encapsulated in nitrogen-doped graphene	0.01-3	200	180	1041	76.4 %	S9
Porous micron-SnO_2/C composites	0.01-3	200	100	954	96 %	S10

References

1. T. Ma, X. Yu, H. Li, W. Zhang, X. Cheng, W. Zhu and X. Qiu, *Nano Lett.*, 2017, **17**, 3959-3964.
2. L. Wang, D. Wang, Z. Dong, F. Zhang and J. Jin, *Nano Lett.*, 2013, **13**, 1711-1716.
3. C. Kim, J. W. Jung, K. R. Yoon, D. Y. Youn, S. Park and I. D. Kim, *ACS Nano*, 2016, **10**, 11317-11326.
4. X. Hu, G. Zeng, J. Chen, C. Lu and Z. Wen, *J. Mater. Chem. A*, 2017, **5**, 4535-4542.
5. J. Qin, N. Zhao, C. Shi, E. Liu, F. He, L. Ma, Q. Li, J. Li and C. He, *J. Mater. Chem. A*, 2017, **5**, 10946-10956.
6. W. Chen, K. Song, L. Mi, X. Feng, J. Zhang, S. Cui and C. Liu, *J. Mater. Chem. A*, 2017, **5**, 10027-10038.
7. Y. Zeng, J. Luo, Y. Wang, L. Qiao, B. Zou and W. Zheng, *Nanoscale*, 2017, **9**, 17576-17584.
8. C. Ma, W. Zhang, Y. S. He, Q. Gong, H. Che and Z. F. Ma, *Nanoscale*, 2016, **8**, 4121-4126.
9. X. Zhou, S. Chen, J. Yang, T. Bai, Y. Ren and H. Tian, *ACS Appl. Mater. Interfaces*, 2017, **9**, 14309-14318.
10. M.-S. Wang, M. Lei, Z.-Q. Wang, X. Zhao, J. Xu, W. Yang, Y. Huang and X. Li, *J. Power Sources*, 2016, **309**, 238-244.